Large tissue archiving solution for multiplexed labeling and super-resolution imaging

Ya-Hui Lin[1,2], Li-Wen Wang[1,2], Yen-Hui Chen[3], Yi-Chieh Chan[1], Shang-Hsiu Hu[1], Sheng-Yan Wu[1], Chi-Shiun Chiang[1], Guan-Jie Huang[2,4], Shang-Da Yang[2,5], Shi-Wei Chu[2,4], Kuo-Chuan Wang[6], Chin-Hsien Lin[7], Pei-Hsin Huang[8], Hwai-Jong Cheng[9], Bi-Chang Chen[10,*] & Li-An Chu[1,2,*]

1. Department of Biomedical Engineering and Environmental Sciences, National Tsing Hua University, Hsinchu, Taiwan
2. Brain Research Center, National Tsing Hua University, Hsinchu, Taiwan
3. Institute of Biomedical Sciences, Academia Sinica, Taipei, Taiwan
4. Department of Physics, National Taiwan University, Taipei, Taiwan
5. Institute of Photonics Technologies, National Tsing Hua University
6. Department of Neurosurgery, National Taiwan University Hospital, College of Medicine, National Taiwan University, Taipei, Taiwan
7. Department of Neurology, National Taiwan University Hospital, College of Medicine, National Taiwan University, Taipei, Taiwan
8. Department of Pathology, National Taiwan University Hospital, Taipei, Taiwan
9. Institute of Molecular Biology, Academia Sinica, Taipei, Taiwan
10. Research Center for Applied Sciences, Academia Sinica, Taipei, Taiwan

Abstract

Tissue clearing and expansion microscopy have significantly advanced neuroscience by enabling the visualization of spatial information about biological components, from tissue-level architecture to nanoscale structures. Currently, their application is limited to tissues without prolonged fixation, which excludes long-term preserved specimens, such as human brains. To address this issue, we present a new multiplex labeling and expansion-applicable method for centimeter-sized archived tissue (MOCAT). We successfully applied MOCAT to formalin-fixed paraffin-embedded (FFPE) mouse, pig, and human brain blocks up to 15 years old. The reliability of MOCAT was demonstrated by the indistinguishable spatial and quantitative information of biomarkers obtained from FFPE intact mouse brains compared to that from freshly prepared SDS-delipidated intact mouse brains. Additionally, MOCAT-processed FFPE samples exhibited superior long-term antigenicity preservation and suitability for advanced expansion microscopy in human brain compared to those kept in 10% formalin. In summary, MOCAT combined with FFPE fulfills the demand for long-term tissue preservation and organ-level multiplex imaging in super-resolution.

Introduction

The fact that the brain functions as an organic entirety necessitates whole-brain imaging in neuroscientific or clinical brain research. This requirement may be fulfilled by the recent advancements in tissue clearing techniques[1–8]. Tissue clearing techniques combined with deep-immunolabeling[9–12] and genetic tools[13] capable of labeling specific proteins, cells, or neurons enable volumetric imaging of an intact mouse brain and provide brain-wide information that cannot be obtained from conventional histological approaches[14–17]. However, current tissue clearing approaches did not suggest an appropriate way to preserve samples that need to be archived for future three-dimensional (3D) or super-resolution imaging. Human brain banks usually archive precious human tissues in formalin or ultra-low temperature freezers. However, both ways have their drawbacks. Long-term formalin preservation causes stable crosslinks and over-occupied amine groups that hinder immunolabeling[18] and modern technologies such as expansion microscopy[19], and thawing of frozen biological samples can cause cellular damage due to the formation of ice crystals during freezing and subsequent thawing-induced stresses on the cellular structure. This limitation makes researchers opt for tissue sections and contradicts research using archived human brains. Therefore, a new method is required to bridge the gap between the need for long-term tissue preservation and further organ-level multiplex imaging in cellular or even in super-resolution.

Paraffin embedding is a standard tissue archiving technique commonly used in clinical and research laboratories. Biological samples can be dehydrated and preserved in formalin-fixed paraffin-embedded (FFPE) blocks for years at room temperature without the concern of over-fixation. The proteomic information can be preserved in pristine condition[20]. Some studies have performed tissue-clearing methods such as CUBIC[21], iDISCO[22–24], CLARITY[25] and passive SDS-treatment[26] on thin FFPE sections. In these studies, FFPE samples were dewaxed and then treated in the same way as standard formalin-fixed tissues for delipidation, and only up to 1~2 mm deep immunolabeling was achieved. To develop an approach for centimeter-level FFPE tissue clearing and immunolabeling, we took two features of FFPE tissue that formalin-fixed tissues do not possess into consideration. First, a significant amount of lipids in FFPE tissues have been removed by xylene during paraffin embedding and dewaxing. Second, proteolytic or heat-induced epitope retrieval[27] is usually necessary before immunohistochemistry on FFPE tissue sections to unmask crosslinked antigens. Here, we present multiplex labeling of centimeter-sized archived tissue (MOCAT), a delipidation and multiplex immunolabeling approach designed for FFPE brains. First, we demonstrated that MOCAT

enables multiple rounds of immunolabeling and works on old FFPE blocks. Second, we applied MOCAT on brains collected from traumatic brain injury mice and demonstrated that FFPE brains preserve the same proteomic information as formalin-fixed brains. Third, we demonstrated that FFPE is superior to 10% formalin for long-term antigenicity preservation and advanced expansion microscopy. Finally, we have proved that FFPE and MOCAT can be applied to enormous specimens such as whole pig brains, ensuring future application in human samples.

Results

Development of MOCAT

Although xylene removed a significant amount of lipids during FFPE, studies have indicated that phospholipids and myelinated lipids are retained after FFPE processing and dewaxing possibly due to crosslinking with surrounding proteins[28]. Thus, theoretically, the step of antigen retrieval that unmasks crosslinked epitopes would help release protein-linked lipids. Therefore, we sought to design a new antigen retrieval (AR) protocol that also removes residual lipids from dewaxed FFPE brains. Our strategy was optimizing detergent conditions (including concentration and detergent types) of heat-induced epitope retrieval (HIER) and utilizing the high temperature of HIER to reinforce detergent into tissues and accelerate delipidation. Serial concentrations of tween 20 and four other detergent candidates were mixed into citrate buffer (10mM Sodium Citrate, pH 6.0) individually (see methods for details). Two of the detergents (triton X-100, tween 20) have been commonly used to penetrate cells in immunohistochemistry, and the other three (SDS, CHAPS and sodium cholate) have been used in published tissue clearing methods[29–31]. We then performed the clearing tests on 2-mm-thick FFPE brain slices, respectively, and each brain slice was further immunolabeled with NeuN (a neuronal nuclear marker) and SMI312 (a pan-neurofilament marker) antibodies. We found that no NeuN signal was observed in the brain slices treated with 1% sodium cholate (NaC) or 1% CHAPS, indicating unsuccessful antigen retrieval (Fig. 1a); the brain slices treated with citrate buffer containing no detergent or 0.1% Tween 20 showed neuronal nuclear signals, but the faint signals at 1-mm depth implied the opacity due to insufficient delipidation; the brain slice treated with 1% Tween 20 showed sharp and clear neuronal nuclei and axon bundles with low background fluorescence, suggesting the dose-dependent improvement of delipidation. The brain slice treated with 1% SDS also resulted in an excellent signal-to-background ratio (Fig. 1a); however, the brain slice turned expanded and fragile after heat-SDS treatment (Supplementary Fig. 1). Therefore, we opted to use 1% Tween 20 in the modified HIER. We termed this versatile delipidation/antigen

retrieval method MOCAT (Multiplex labeling Of Centimeter-sized Archived Tissue) (Fig 1b).

To verify the delipidation efficiency of MOCAT, we adopted coherent anti-Stokes Raman scattering (CARS), a spectroscopic technique used to detect vibrational responses of specific molecular structures, to assess the remained lipid amount of mouse brain samples (Fig. 1c). We observed the CARS signal of axon bundles in the dewaxed FFPE mouse brain (Fig. 1c, left), indicating myelinated lipids existence. Conversely, the CARS signal was not observed after MOCAT (Fig. 1c, middle), indicating the removal of myelinated lipids. We also found that the CARS images of the dewaxed FFPE mouse brain after MOCAT and the 24-hour 4% paraformaldehyde (PFA) fixed SDS-delipidated exhibited similar average gray-level values (Fig. 1c middle and right), indicating similar delipidation abilities of the two procedures. The results suggested that MOCAT could be used to delipidate dewaxed FFPE brains sufficiently.

MOCAT reveals protein spatial information for 3D visualization of FFPE brain tissue blocks

Next, we applied MOCAT to an intact FFPE mouse brain and performed immunolabeling with tyrosine hydroxylase (TH, a dopaminergic neuronal marker) antibodies to demonstrate the intact Dopaminergic neuronal map in FFPE brain tissues. To speed up immunolabeling and protect samples from the harsh conditions of multiplexed staining, we combined the stabilization to harsh conditions via intramolecular epoxide linkages to prevent degradation (SHIELD) procedure[32] and electrophoretic immunolabeling[11] into the MOCAT pipeline (Fig. 1b). In the FFPE mouse brain, dopaminergic neuronal distribution was clearly revealed in the striatum, nigrostriatal fiber tracts, substantia nigra, ventral tegmental area, pontine reticular nucleus, and lateral reticular nucleus (Fig. 1d, right). The distribution pattern was identical in the 24-hour 4% PFA fixed SDS-delipidated (hereinafter referred to as SDS-delipidated) mouse brain (Fig. 1d, left), demonstrating that MOCAT enables the comparable 3D visualization of an intact mouse brain to an SDS-delipidated brain. These results also suggest that FFPE brains preserve spatial information comparable to 24-hour PFA-fixed brains.

To examine if MOCAT could be applied to aged specimens, we applied this method to a 15-year-old, 2-mm-thick FFPE block (Fig. 1e). The brain regions containing dopaminergic neurons were identified (Fig. 1f), and the morph of individual dopaminergic neurons was observed (Figs. 1g). These results suggest that three-dimensional (3D) expression patterns of biological markers could be preserved for decades and revealed later by performing MOCAT. Notably, the dewaxing time should be increased when working with a large sample; otherwise, the residual wax from insufficient dewaxing would cause

115 opacity. The opacity could be removed through repeated dehydration and dewaxing
116 (Supplementary Fig. 2b), and repeated dewaxing and prolonged dewaxing time did not
117 affect tissue structure or antigenicity (Supplementary Figs. 2 and 3).
118

119 MOCAT enables multiplexed immunolabeling of an FFPE tissue block

120 Multiplex immunostaining is essential to further investigating molecule interactions and
121 the microenvironment. However, the number of biological markers labeled in a single
122 round is typically limited by antibody host species and the fluorescent
123 excitation/emission wavelength spectrums. To overcome this limitation, we included a
124 step for multiple rounds of immunostaining in the MOCAT pipeline (Fig. 1c). To maintain
125 the fluorescent signals, we postfixed the labeled sample with 4% PFA after each round of
126 immunolabeling (Supplementary Fig. 4). After imaging completed, the RI-matched
127 transparent sample was photo-bleached by LED white light. To release the re-masked
128 epitopes by the post-immunolabeling fixation, we performed another round of HIER (Fig.
129 2a and Supplementary Fig. 5) before the next round of immunolabeling. Repeating the
130 steps, we performed six continuous rounds of immunolabeling on the same
131 MOCAT-treated FFPE mouse brain. For each round, the brain was labeled with lectin as a
132 structural reference and one antibody specific for a target protein (Fig. 2b). The six
133 antibody image data sets were then registered and aligned using Elastix[33] to generate a
134 multichannel image (Fig 2c). These results demonstrated the applicability of MOCAT to
135 FFPE tissues for revealing the spatial distribution of different neuronal markers and the
136 compatibility of MOCAT with various primary antibodies.
137

138 The protein expression changes caused by disease and therapy are 139 preserved in FFPE blocks and retrieved by MOCAT

140 Volumetric imaging is vital for disease research because it offers precise
141 microenvironment spatial information and therapy effect evaluation[17,25,34]. To examine
142 the applicability of MOCAT to disease research, we first applied MOCAT to an FFPE
143 mouse brain of the astrocytoma mouse model (see Methods) to label the tumor cells
144 and astrocytes (Fig. 3a and c). Astrocytes surrounding the tumor were segmented (Fig.
145 3b, d and e) and classified by their cell-to-tumor distances. The statistics (Fig. 3f) showed
146 that almost half of the astrocytes were inside the tumor, while 63.9% were near the
147 tumor surface (within ± 200 µm). Our results showed that the image data sets of MOCAT
148 can be used to analyze cell distribution and reveal the spatial architecture of a disease
149 microenvironment. We then used a mouse model of traumatic brain injury (TBI) to
150 compare the quantification results of MOCAT-processed and SDS-delipidated mouse
151 brains. Studies have reported that TBI disrupts dopamine neurotransmission, reduces
152 dopamine levels, and causes cell loss in the nigrostriatal system[35,36]. Therefore, we use

153 TH antibodies to label the dopaminergic system (Fig. 4a). We found that the injury side
154 of the brain showed striatal morphological extension and distortion in both
155 SDS-delipidated (Supplementary Fig. 6) and MOCAT (Fig. 4b) processed samples,
156 implying a possible malfunction or imbalance in the dopaminergic system. To assess the
157 damage, we segmented the striatum (Fig. 4b), nigrostriatal fiber tracts (Fig. 4c) and the
158 dopaminergic neuronal cells in the substantia nigra (Fig. 4d) and calculated the relative
159 volumes and cell numbers of the injury side to the contralateral side. We found that the
160 injury side of both MOCAT and SDS-delipidated TBI brain showed approximately 20%,
161 30%, and 15% reduction in striatal volume, nigrostriatal fiber tract volume, and cell
162 number of substantia nigra, respectively, compared to the contralateral side (Fig. 4e),
163 indicating that neuronal damage was preserved and could be assessed using FFPE
164 samples. Next, we evaluated the therapeutic effect of a nitrogen oxide-producing
165 nanoparticle (aNORO, See Methods) on angiogenesis. We segmented an area of blood
166 vessels directly beneath the injury site of both sham and aNORO-received mouse brains
167 (Fig. 4f and Supplementary Fig. 7) and calculated the volume, surface area, length, and
168 the number of bifurcations to assess angiogenesis (see Methods). The results of both
169 MOCAT and SDS-delipidated brains indicated that the mouse receiving aNORO injection
170 exhibited approximately 60% improvement in angiogenesis compared to the sham group
171 (Fig. 4g). Taken together, we demonstrated that the structural and proteomic
172 expressional changes can be preserved in FFPE tissues; this information could be
173 revealed via MOCAT and makes the archived tissues usable to evaluate therapeutic or
174 behavioral experimental effects.
175

176 FFPE is superior to formalin in archiving human brain tissues for 3D 177 visualization and advanced super-resolution microscopy

178 While long-term archiving mouse brains for future intact imaging is still new, human
179 brain sample preservation has been performed in human brain tissue banks worldwide.
180 In most research centers, collected tissues are stored unfixed at −70ºC to −85ºC or in
181 10% formalin at room temperature. However, ultralow temperature preservation leads
182 to structural destruction caused by impetuous thawing, and strong crosslinks caused by
183 long-term storage in formalin impede aqueous-based delipidation[18,26] and reduce tissue
184 antigenicity[37], preventing scientists from 3D visualization. To demonstrate the
185 superiority of FFPE for tissue preservation, we applied MOCAT to an FFPE human brain
186 tissue sample collected surgically from the temporal lobe and compared
187 immunolabeling results with the results of formalin-preserved brain blocks stored for 1
188 year and 45 days (see Methods). The astrocytic foot processes were stained in the brain
189 specimen stored in an FFPE block for 60 days but not in the formalin-preserved brain
190 blocks stored for 1 year and 45 days (Fig. 5a), indicating that FFPE is superior to formalin

for antigenicity preservation. On the same sample, we then performed two additional rounds of immunolabeling to axons and dendrites, respectively (Supplementary Fig. 8). The image data sets from each round could be registered into a single multichannel image with lectin-labeled blood vessels as a reference channel (Fig. 5b), enabling us to reconstruct the relationship between these biomarkers.

Expansion microscopy[38,39] is a technique used in super-resolution microscopy to surpass the limitations of optical diffraction by enlarging biological structures. This is achieved by a polymer network synthesizing within the specimen to anchor protein molecules, causing the specimen to expand physically and enabling researchers to study sub-cellular structures. However, formaldehyde-induced crosslinks may impede the effectiveness of expansion microscopy[40,41]. To address this issue, specimens preserved with 4% PFA for 24 hours before paraffin processing are suggested to yield higher quality results compared to those preserved solely in formalin. To test this hypothesis, FFPE human brain specimens and specimens preserved in formalin for one year were subjected to the 4x expansion protocol. The results showed that FFPE brain tissue underwent successful expansion (Fig. 5c, bottom row), resulting in sharper and clearer images (Fig. 5d), while the 1-year formalin-fixed brain tissue remained opaque and showed distortion (Fig. 5d, upper row). Therefore, FFPE is a preferable preservation method for 3D visualization and expansion microscopy.

To evaluate the maximum sample size that the FFPE and MOCAT can accommodate, we employed pig brains and performed paraffin processing (Supplementary Fig. 9). After embedding, the block was cut open to examine the paraffin penetration. There were no bubbles or holes inside the embedded brain (Supplementary Fig. 9d-f), indicating excellent paraffin penetration. These results suggested the feasibility of preserving an intact human brain in an FFPE block.

Discussion

This study presents a versatile technique MOCAT that combines tissue clearing and antigen retrieval for whole-tissue immunolabeling and following volumetric imaging or expansion microscopy of archived or achieve-ready brain tissues. Some studies have performed tissue-clearing on FFPE specimens[21–24,26,42], but they only considered FFPE tissues as a specimen type. No attempt has been made to exploit the characteristics of FFPE processing in large tissue clearing. Surprisingly, in these studies, antigen retrieval had not been included in the workflow of whole-tissue immunolabeling. It is probable that tissue clearing, such as SDS-electrophoresis, also possesses minor antigen retrieval

229 ability. In our preliminary tests, the SDS-delipidated FFPE mouse brain (without heat
230 treatment) exhibited visible but weak dopaminergic signals and noticeable nonspecific
231 background noises (Supplementary Fig. 10c) that have been observed in FFPE tissue
232 sections with inadequate antigen retrieval[30], implying the partial antigen retrieval effect
233 of SDS-delipidation. These results also indicated that heat-induced antigen retrieval is a
234 crucial step that cannot be replaced by delipidation at room temperature. We also
235 tested using Tris-EDTA instead of citrate buffer in MOCAT. We found that both groups
236 have satisfying immunolabeling results (Supplementary Fig. 10e and f), suggesting that
237 the primary buffer (citrate buffer or Tris-EDTA) could be chosen according to antibody
238 preference without affecting the delipidation effect.
239
240 One of the significant advantages of FFPE is convenient storage without the concern of
241 over-fixation. Over-fixation due to long-term formalin storage has been proved to cause
242 many experimental difficulties; however, many hospitals and institutes still keep precious
243 human brains in formalin instead of paraffin; one of the reasons probably is the
244 enormous size of the human brain. In this study, we demonstrated that an entire pig
245 brain could be processed using a tissue processor and embedded in paraffin with
246 sufficient penetration. The result indicated the possibility of archiving huge-sized human
247 brains in paraffin blocks for future research.
248
249 Although MOCAT was designed for FFPE brains, it can also work as a fast,
250 high-throughput delipidation method by combining with serial dehydration, xylene
251 clearing and rehydration. Compared with other organic solvent-based large tissue
252 clearing methods, such as 3DISCO and iDISCO, MOCAT processing is easier to perform in
253 hospitals and research institutes, and the necessary solvents (ethanol and xylene) are
254 less expensive and more readily available. Though it has been reported that endogenous
255 fluorescent proteins are easily quenched in ethanol[9], they can still be visualized through
256 immunolabeling.
257
258 MOCAT is applicable to aged FFPE blocks and enables repeated immunolabeling on the
259 same specimen, compensating for the rarity of clinical human brain specimens.
260 Therefore, MOCAT is a powerful tool for clinical brain research, including the
261 investigation of the microenvironment surrounding lesions. To achieve this purpose, we
262 require computational tools to register and align multiplex data sets. The published tools,
263 such as Advanced Normalization Tools (ANTs)[43] and Elastix[33], are suitable for use in
264 specimens with clear boundaries, such as intact mouse brains. However, the registration
265 could be better for a patient-obtained piece of human brain tissue, which typically has
266 broken boundaries and irregular shapes. Therefore, developing an algorithm for

267 registering large-size data sets from irregularly shaped samples is essential for future
268 volumetric human brain imaging.
269
270 The strong autofluorescence caused by blood cells and lipofuscin is another challenge
271 for 3D visualization of a human brain sample. Protocols reported being effective on
272 tissue sections to eliminate the auto-fluorescence, such as $CuSO_4$[44] and
273 photobleaching[45], only weaken the autofluorescence in large human tissue in our hands.
274 Some studies have used H_2O_2[46], which is unsuitable for large tissue because prolonged
275 immersion time may affect antigenicity. An alternative method utilizing spectral imaging
276 and linear unmixing was reported for identifying and removing autofluorescence in brain
277 tissue sections[47]; this method has the potential to be modified and applied to large
278 tissues.
279
280 In conclusion, MOCAT efficiently delipidates and retrieves epitopes from FFPE brain
281 tissues. Combined with FFPE preservation, MOCAT provides a solution for archiving
282 biological samples for future whole-mount immunolabeling and 3D visualization. MOCAT
283 also maximizes the use of archived tissues and facilitates future studies in 3D mappings,
284 such as connectomics.
285
286
287 **Methods**
288
289 Experimental animals and human samples
290 We used 8-week-old CD-1 male mice for the MOCAT pipeline development. All animal
291 procedures and handlings complied with the guideline from the Institutional Animal
292 Care and Use Committee of Academia Sinica (IACUC protocol No.: 12-05-370), Taiwan.
293 Experimental mice information for astrocytoma and TBI mouse models is described
294 below. The postmortem human brain samples were provided by Dr. Hwai-Jong Cheng.
295 The studies involving human participants were reviewed and approved by the
296 Institutional Review Board of National Taiwan University Hospital (IRB No.:
297 202203079RINC), and the participants provided signed informed consent.
298
299 Astrocytoma animal model
300 All animal procedures and handlings complied with the guideline from the Institutional
301 Animal Care and Use Committee of National Tsing Hua University (IACUC protocol No.:
302 109067), Taiwan. ALTS1C1-GFP cells (1×10^5 cells) were implanted into the brains of
303 8-week-old C57BL/6 mice following the procedure published[48]. Briefly, under anesthesia,
304 1×10^5 ALTS1C1-GFP cells were injected with a 2.5-mm depth at 2 mm laterals to the

305 midline and 1 mm posterior to the bregma. After injection, bone wax (ETHICON, W810,
306 Somerville, NJ, USA) was applied to seal the drilled hole. Eighteen days after the tumor
307 implantation, mice were sacrificed after cardiac perfusion.
308

309 TBI mouse model

310 All animal procedures and handlings complied with the guideline from the Institutional
311 Animal Care and Use Committee of National Tsing Hua University (IACUC protocol No.:
312 110081). We divided 7-week-old C57BL/6 female mice into two groups: (1) untreated
313 (sham) and (2) treated with alternating magnetic field-responsive NO-release
314 octahedrons (aNORO@sMN). When applying TBI to mice, we used an electric drill to
315 create a hole in the skull. The TBI site was on the left motor cortex (M1 & M2). A
316 2-mm-diameter punch was then used to cause a 1.5-mm-deep injury. For the treated
317 group, the NO-release octahedrons (aNORO) were embedded in a silk microneedle
318 (sMN). The microneedle was implanted one day postinjury to avoid excessive swelling in
319 the injured area. The mice were sacrificed 45 days after the TBI induction.
320

321 MOCAT

322 The MOCAT workflow is presented in Fig. 1b. The details are provided below.
323

324 *Sample preparation.* For the mouse brains, mice were perfused with 20 mL of cold
325 phosphate-buffered saline (PBS) and then 20 mL of 4% PFA. The collected brains were
326 further fixed using 4% PFA at 4°C for 24 hours. For the human brain specimens, human
327 brain tissues were collected surgically from the temporal lobe of patients and fixed with
328 4% PFA at 4°C for 24 hours. The PFA-fixed specimens were dehydrated, processed in a
329 tissue processer (The Tissue-Tek VIP 5 Jr., Sakura Finetek Japan Co., Ltd., Japan), and
330 embedded in paraffin wax. The FFPE blocks were stored at room temperature.
331

332 *Deparaffination and rehydration.* The FFPE brains were incubated at 65°C to melt
333 paraffin. Residual paraffin was removed through immersion in xylene for 24 hours.
334 Xylene was changed at least twice. Dewaxed brains were rehydrated with 100%, 100%,
335 95%, 85%, 75%, and 55% alcohol diluted with distilled water. The rehydrated brains were
336 then washed with PBS.
337

338 *SHIELD procedure.* The dewaxed and rehydrated brains were treated with epoxy
339 following the published SHIELD protocol[32]. The brains were incubated in the SHIELD-OFF
340 solution at 4°C for four days, followed by one more day in the SHIELD-ON solution at
341 37°C. All reagents were prepared from SHIELD kits (LifeCanvas Technologies, Seoul,
342 South Korea) according to the manufacturer's instructions.

343

344 *Antigen retrieval.* The SHIELD-processed brains were incubated overnight at 37°C in a
345 modified citrate buffer (10 mM sodium citrate, 1% Tween 20, pH 6.0). The brains and
346 buffer were then cooked for 10 min at 121°C in a pressure cooker (Bio SB, Santa Barbara,
347 CA, USA). The brains and buffer were kept in the pressure cooker until the temperature
348 dropped below 100°C (for approximately 15 min). Next, the brains were removed from
349 the cooker and allowed to cool for 10 min at room temperature. The brains were then
350 washed in PBST (1× PBS with 0.1% Triton X-100) 3 times, with 1 hour per wash.

351

352 *Electrophoretic immunolabeling.* The procedure was modified from the published
353 eFLASH protocol[11] and conducted in the SmartLabel System (LifeCanvas Technologies,
354 Seoul, South Korea). The brains were preincubated overnight at room temperature in
355 sample buffer (240 mM Tris, 160 mM CAPS, 20% w/v D-sorbitol, 0.9% w/v sodium
356 deoxycholate). Each preincubated brain was placed in a sample cup (provided by the
357 manufacturer with the SmartLabel System) containing primary and corresponding
358 secondary antibodies diluted in 8 mL of sample buffer. Antibody information and
359 optimized quantity are detailed in Supplementary Table 1. The sample cup and 500 mL
360 of labeling buffer (240 mM Tris, 160 mM CAPS, 20% w/v D-sorbitol, 0.2% w/v sodium
361 deoxycholate) were loaded into the SmartLabel System. The device was operated at a
362 constant voltage of 90 V with a current limit of 400 mA. After 18 hours of
363 electrophoresis, we added 300 mL of booster solution (20% w/v D-sorbitol, 60 mM boric
364 acid), and electrophoresis was continued for 4 hours. Immunolabeled brains were
365 washed with PTwH[9] (1× PBS with 0.2% w/v Tween-20 and 10 μg/mL heparin) 2 times,
366 with 3 hours per wash, and then postfixed with 4% PFA at room temperature for 1 day.
367 The brains were washed with PBST 2 times, with 3 hours per wash, to remove any
368 residual PFA.

369

370 *Refractive index (RI)-matching.* Before imaging, the brains were RI-matched by
371 immersing them in NFC1 and NFC2 solutions (Nebulum, Taipei, Taiwan) for 1 day at room
372 temperature.

373

374 *Volumetric imaging and 3D visualization.* The whole mouse brain was imaged using a
375 light-sheet microscope (SmartSPIM, LifeCanvas Technologies, Seoul, South Korea). For
376 less-than-3-mm-thick samples, imaging was performed using a multipoint confocal
377 microscope (Andor Dragonfly 200, Oxford Instruments, UK). 3D visualization was
378 performed using Imaris software (Imaris 9.5.0, Bitplane, Belfast, UK).

379

380 *Photobleaching.* The immunolabeled and imaged brain was placed in a multiwell plate

381 and immersed in RI-matching solutions to keep it transparent. The plate was sealed with
382 paraffin. A 100-W projection lamp with an LED array was placed on the plate to quench
383 the fluorescent signals. A representative photobleaching apparatus constructed using
384 off-the-shelf components is shown in Supplementary Fig. 11. For a 2-mm-thick sample,
385 18 hours of photobleaching was sufficient.
386

387 ## Detergent condition test

388 2-mm thick mouse brain slices were FFPE processed, dewaxed and rehydrated, and
389 SHIELD processed as described in the MOCAT section of Methods. Processed brain slices
390 were incubated overnight at 37°C in citrate buffer (10 mM sodium citrate, pH 6.0) with
391 various detergent conditions (no detergent, 0.1% Tween 20, 1% Tween 20, 1% Triton
392 X-100, 1% CHAPS, 1% sodium cholate, 1% SDS). Brain slices were then cooked and
393 immunolabeled with NeuN and SMI312 antibodies as described in the MOCAT section.
394

395 ## SDS-delipidation

396 The mice were perfused with 20 mL of cold phosphate-buffered saline (PBS) and then 20
397 mL of 4% PFA. The brains were collected and further fixed in 4% PFA at 4°C for 24 hours.
398 The fixed brains were treated with SHIELD procedure described in previous session. The
399 SHIELD-processed brains were cleared using stochastic electro-transport (SmartClear Pro
400 II, LifeCanvas Technologies, Seoul, South Korea) with a constant current 1.2 A for 5-7
401 days. The cleared brains were washed with PBST (1X phosphate-buffered saline
402 containing 0.1% triton X-100 detergent) at room temperature for at least overnight.
403

404 ## Raman microscopy

405 A Yb:KGW laser (Carbide, Light Conversion) emitting 190 fs, 200 kHz, 20 W pulse train at
406 1030 nm wavelength is used to generate supercontinuum via a double-pass
407 multiple-plate continuum module[49]. The resulting spectrum (600-1300 nm) is spectrally
408 sliced by tunable color filters (3G LVLWP, LVSWP, and LVFBP, Delta) to provide pump (725
409 nm) and Stokes (914 nm) beams, which can address the Raman shift (2850 cm^{-1}) of lipids.
410 The two beams are temporally and spatially overlapped, then guided into a commercial
411 upright microscope (Axio Examiner.Z1, Zeiss) with a scanning unit (LSM7MP, Zeiss) to
412 achieve raster scanning on the x-y plane. A single 20x water immersion objective
413 (UMPLFLN 20XW, Olympus) is used to focus the combined laser beams on the mouse
414 sample. Epi-CARS signal at 601 nm is spectrally separated from the incident radiation
415 with a bandpass filter (BP 565-610, Zeiss) and detected by a photomultiplier tube. The
416 mean gray value is calculated via ImageJ.
417

418 ## Multichannel image registration

419 For the 6-round immunolabeling of a single whole mouse brain, the data sets of each
420 round contain one structural channel stained with lectin and one antibody-stained
421 channel. The image data set of the first staining round was used as a standard brain. The
422 lectin channel images of each other data set were registered to the lectin channel of the
423 standard brain through Elastix toolbox[33]. Transformation parameters obtained from rigid
424 and B-spline deformable registration were applied to the antibody-stained channels.
425 Transformed images were merged and visualized using Imaris software. For the human
426 specimen, the image data sets of three rounds were registered and resampled using
427 Amira software (Thermo Fisher Scientific, Waltham, MA, USA). Resampled images were
428 merged and visualized using Imaris software.
429

430 ## Quantification and statistics

431 For volume and surface area quantification, we used the Surface function of Imaris
432 software to segment the striatum, nigrostriatal fiber tracts, and blood vessels in the
433 selected regions of interest. For cell number quantification, the area of substantia nigra
434 (SN) was masked out using Surface, and the cells within SN were detected using the Spot
435 function of Imaris. For calculating the bifurcations and length of blood vessels, we used
436 the feature extraction method provided by Vessap[50] to detect the centerlines of the
437 blood vessels and the bifurcation point. First, erosion and dilation were performed to
438 remove false-negative pixels and avoid false centerline detections. Next, the centerlines
439 were extracted with a 3D thinning algorithm[51], and the bifurcation points were detected
440 using the surrounding pixels of each point to decide a point that splits into two or more
441 vessels. All statistical analyses were performed using GraphPad Prism (GraphPad
442 Software Inc., San Diego, CA, USA).
443

444 ## Expansion microscopy of FFPE and 1-year formalin-fixed human specimens

445 Expansion microscopy was performed following a modified 4x proExM[39] protocol. FFPE
446 human specimens were dewaxed and rehydrated as described in MOCAT section of
447 Methods. The processed FFPE human specimen and the specimen fixed with formalin
448 for 1 year were incubated in anchoring solution (0.01% w/v methacrylic acid
449 N-hydroxysuccinimide ester in 1×PBS) at 4°C for 24 hours. After anchoring, samples were
450 washed twice with PBS at room temperature for 5 minutes each, and then rinsed twice
451 in acrylamide monomer solution (2 M NaCl, 8.625% w/w sodium acrylate, 2.5% w/w
452 acrylamide, 0.15% w/w N,N'-methylenebisacrylamide in 1×PBS) at 4°C for 5 minutes
453 each. For gelation, specimens were pre-incubated in gelation solution (0.02% w/w
454 ammonium persulfate (APS), 0.02% w/w tetramethyl- ethylenediamine (TEMED) and
455 0.01% w/w 4-hydroxy-2,2,6,6-tetrameth- ylpiperidin-1-oxyl (4-hydroxy-TEMPO) in
456 monomer solution) for 5 min at 4°C, and then moved into fresh gelation solution for

457 additional 25 min. The specimen with gelation solution were then transferred to a
458 humidified 37 °C incubator for 2 hours. The gels were then immersed in protease
459 digestion solution (8 units/ml protease K, 50 mM Tris (pH 8.0), 0.8 M guanidine
460 hydrochloride, 0.5% w/v Triton X-100, 2 mM calcium chloride) at room temperature for
461 18-20 hours. After digestion, the gels were immersed in an excess of deionized water for
462 0.5-2 hours to expand. This step was subsequently repeated 3–5 times with fresh water
463 until the size of the sample stopped increasing. For post-expansion immunolabeling, the
464 digested gels were washed in PBS twice for 20 minutes each, and incubated in primary
465 antibody cocktail containing anti-SMI312 (Biolegend, 837904, 1:500 dilution) anti-MAP2
466 (Cell signaling technology, #8707, 1:500 dilution), normal goat serum (Jackson
467 ImmunoResearch, 005-000-121, 1:500 dilution) and 0.1% w/v Triton X-100 in 1×PBS at
468 4°C for 24 hours. Gels were then washed in wash buffer (30 mM sodium chloride, 0.1%
469 w/v Triton X-100 in 1×PBS) 3 times for 20 minutes each and incubated in secondary
470 antibody cocktail containing Alexa Fluor® 647 AffiniPure goat anti-mouse IgG (Jackson
471 ImmunoResearch, 115-605-003, 1:500 dilution), Rhodamine Red™-X (RRX) AffiniPure
472 goat anti-rabbit IgG (Jackson ImmunoResearch, 111-295-003, 1:500 dilution), normal
473 goat serum and 0.1% w/v Triton X-100 in 1×PBS at 4°C for 24 hours. The
474 antibody-labeled gels were washed in wash buffer 3 times for 20 minutes each, and then
475 placed in deionized water for expansion. For nuclei staining, propidium iodine were
476 added in deionized water at a final concentration of 1μg/ml during expansion.
477

478 ## FFPE processing of whole pig brains

479 Pig brains were obtained from market and immersed in PFA/alcohol solution (2% w/v
480 PFA in 50% alcohol) within two hours after slaughter. The pig brains were fixed in
481 PFA/alcohol solution for 12 hours, and then transferred to 4% PFA and incubated at 4°C
482 for 48 hours. The fixed pig brain were rinsed with PBS to remove excess PFA, and
483 processed in a tissue processer (The Tissue-Tek VIP 5 Jr., Sakura Finetek Japan Co., Ltd.,
484 Japan) using following procedure: 50% alcohol, 70% alcohol, 80% alcohol, and 95%
485 alcohol for four hours each, three times in 100% alcohol for four hours each, and three
486 times in xylene and paraffin for four hours each, in vacuum and slow mix mode. The
487 processed pig brain were then embedded in paraffin.
488

489 ## Antigen retrieval test

490 Mouse brains were collected, FFPE processed, dewaxed and rehydrated, and SHIELD
491 processed as described in the MOCAT section of Methods. For the antigen retrieval step
492 before immunolabeling, five conditions were tested: (1) No antigen retrieval; (2) SDS at
493 room temperature; (3) Heat-induced retrieval in citrate buffer (pH 6.0) with 0.1% Tween
494 20; (4) Heat-induced retrieval in citrate buffer (pH 6.0) with 1% Tween 20; (5)

495 Heat-induced retrieval in Tris-EDTA buffer (pH 9.0) solution with 1% Tween 20. For
496 condition 1, the dewaxed, SHIELD-processed brain directly proceeded to the
497 immunolabeling step. For condition 2, SDS-based electrophoresis was performed using
498 stochastic electrotransport (SmartClear Pro II, LifeCanvas Technologies, Seoul, South
499 Korea) with a constant current of 1.2 A for 2 days. For condition 3 and 4, the dewaxed,
500 SHIELD-processed brain was incubated overnight at 37°C in citrate buffer (10 mM
501 sodium citrate, pH 6.0) containing 0.1 and 1% Tween 20 respectively. The brains and
502 buffer were then cooked for 10 min at 121°C in a pressure cooker (Bio SB, Santa Barbara,
503 CA, USA). Finally, for condition 2, a Tris-EDTA buffer (10mM Tris Base, 1mM EDTA
504 Solution, 1% Tween 20, pH 9.0) was used following the procedure in condition 3 and 4.

References

1. Chung, K. *et al.* Structural and molecular interrogation of intact biological systems. *Nature* **497**, 332–337 (2013).
2. Ertürk, A. *et al.* Three-dimensional imaging of solvent-cleared organs using 3DISCO. *Nat. Protoc.* **7**, 1983–1995 (2012).
3. Tainaka, K. *et al.* Chemical Landscape for Tissue Clearing Based on Hydrophilic Reagents. *Cell Rep.* **24**, 2196-2210.e9 (2018).
4. Ueda, H. R. *et al.* Tissue clearing and its applications in neuroscience. *Nature Reviews Neuroscience* vol. 21 61–79 (2020).
5. Tian, T., Yang, Z. &Li, X. Tissue clearing technique: Recent progress and biomedical applications. *J. Anat.* **238**, 489–507 (2021).
6. Yu, T., Zhu, J., Li, D. &Zhu, D. Physical and chemical mechanisms of tissue optical clearing. *iScience* **24**, 102178 (2021).
7. Kim, S. Y. *et al.* Stochastic electrotransport selectively enhances the transport of highly electromobile molecules. *Proc. Natl. Acad. Sci. U. S. A.* **112**, E6274–E6283 (2015).
8. Hama, H. *et al.* Scale: A chemical approach for fluorescence imaging and reconstruction of transparent mouse brain. *Nat. Neurosci.* **14**, 1481–1488 (2011).
9. Renier, N. *et al.* IDISCO: A simple, rapid method to immunolabel large tissue samples for volume imaging. *Cell* **159**, 896–910 (2014).
10. Murakami, T. C. *et al.* A three-dimensional single-cell-resolution whole-brain atlas using CUBIC-X expansion microscopy and tissue clearing. *Nat. Neurosci.* **21**, 625–637 (2018).
11. Yun, D. H. *et al.* Ultrafast immunostaining of organ-scale tissues for scalable proteomic phenotyping. *bioRxiv* 660373 (2019) doi:10.1101/660373.
12. Susaki, E. A. *et al.* Versatile whole-organ/body staining and imaging based on electrolyte-gel properties of biological tissues. *Nat. Commun. 2020 111* **11**, 1–22 (2020).
13. Navabpour, S., Kwapis, J. L. &Jarome, T. J. A neuroscientist's guide to transgenic mice and other genetic tools. *Neurosci. Biobehav. Rev.* **108**, 732–748 (2020).
14. Roy, D. S. *et al.* Brain-wide mapping reveals that engrams for a single memory are distributed across multiple brain regions. *Nat. Commun. 2022 131* **13**, 1–16 (2022).
15. Roostalu, U. *et al.* Quantitative whole-brain 3D imaging of tyrosine hydroxylase-labeled neuron architecture in the mouse MPTP model of Parkinson's disease. *DMM Dis. Model. Mech.* **12**, (2019).
16. Renier, N. *et al.* Mapping of Brain Activity by Automated Volume Analysis of Immediate Early Genes. *Cell* **165**, 1789–1802 (2016).
17. Liebmann, T. *et al.* Three-Dimensional Study of Alzheimer's Disease Hallmarks Using the iDISCO Clearing Method. *Cell Rep.* **16**, 1138–1152 (2016).
18. Muntifering, M. *et al.* Clearing for Deep Tissue Imaging. *Curr. Protoc. Cytom.* **86**, e38

(2018).
19. Wassie, A. T. &Zhao, Y. Expansion microscopy: principles and uses in biological research. doi:10.1038/s41592-018-0219-4.
20. Shi, S. R. *et al.* Evaluation of the value of frozen tissue section used as 'gold standard' for immunohistochemistry. *Am. J. Clin. Pathol.* **129**, 358–366 (2008).
21. Nojima, S. *et al.* CUBIC pathology: Three-dimensional imaging for pathological diagnosis. *Sci. Rep.* **7**, 1–14 (2017).
22. vanRoyen, M. E. *et al.* Three-dimensional microscopic analysis of clinical prostate specimens. *Histopathology* **69**, 985–992 (2016).
23. Tanaka, N. *et al.* Whole-tissue biopsy phenotyping of three-dimensional tumours reveals patterns of cancer heterogeneity. *Nat. Biomed. Eng.* **1**, 796–806 (2017).
24. Tanaka, N. *et al.* Mapping of the three-dimensional lymphatic microvasculature in bladder tumours using light-sheet microscopy. *Br. J. Cancer 2018 1187* **118**, 995–999 (2018).
25. Chen, Y. *et al.* Three-dimensional imaging and quantitative analysis in CLARITY processed breast cancer tissues. *Sci. Rep.* **9**, 1–13 (2019).
26. Lai, H. M. *et al.* Next generation histology methods for three-dimensional imaging of fresh and archival human brain tissues. doi:10.1038/s41467-018-03359-w.
27. Shi, S. R., Shi, Y. &Taylor, C. R. Antigen retrieval immunohistochemistry: Review and future prospects in research and diagnosis over two decades. *Journal of Histochemistry and Cytochemistry* vol. 59 13–32 (2011).
28. Denti, V. *et al.* Antigen Retrieval and Its Effect on the MALDI-MSI of Lipids in Formalin-Fixed Paraffin-Embedded Tissue. *J. Am. Soc. Mass Spectrom.* **31**, 1619–1624 (2020).
29. Chung, K. *et al.* Structural and molecular interrogation of intact biological systems. *Nature* **497**, 332–337 (2013).
30. Zhao, S. *et al.* Cellular and Molecular Probing of Intact Human Organs. *Cell* **180**, 796-812.e19 (2020).
31. Na, M. *et al.* Sodium Cholate-Based Active Delipidation for Rapid and Efficient Clearing and Immunostaining of Deep Biological Samples. *Small Methods* **6**, (2022).
32. Park, Y.-G. *et al.* Protection of tissue physicochemical properties using polyfunctional crosslinkers. *Nat. Biotechnol.* **37**, 73–83 (2019).
33. Klein, S., Staring, M., Murphy, K., Viergever, M. A. &Pluim, J. P. W. elastix: a toolbox for intensity-based medical image registration. *IEEE Trans. Med. Imaging* **29**, 196–205 (2010).
34. Gómez-Gaviro, M. V., Sanderson, D., Ripoll, J. &Desco, M. Biomedical Applications of Tissue Clearing and Three-Dimensional Imaging in Health and Disease. *iScience* **23**, 101432 (2020).
35. PO, J. *et al.* Dopaminergic abnormalities following traumatic brain injury. *Brain* **141**, 797–810 (2018).

36. Verduzco-Mendoza, A. *et al.* Role of the Dopaminergic System in the Striatum and Its Association With Functional Recovery or Rehabilitation After Brain Injury. *Front. Neurosci.* **0**, 783 (2021).
37. Thavarajah, R., Mudimbaimannar, V. K., Elizabeth, J., Rao, U. K. &Ranganathan, K. Chemical and physical basics of routine formaldehyde fixation. *J. Oral Maxillofac. Pathol.* **16**, 400 (2012).
38. Chen, F., Tillberg, P. W. &Boyden, E. S. Expansion microscopy. *Science (80-.).* **347**, 543–548 (2015).
39. Tillberg, P. W. *et al.* Protein-retention expansion microscopy of cells and tissues labeled using standard fluorescent proteins and antibodies. *Nat. Biotechnol.* **34**, 987–992 (2016).
40. Zhao, Y. *et al.* Nanoscale imaging of clinical specimens using pathology-optimized expansion microscopy. *Nat. Biotechnol. 2017 358* **35**, 757–764 (2017).
41. Bucur, O. *et al.* Nanoscale Imaging of Clinical Specimens Using Conventional and Rapid Expansion Pathology. *Nat. Protoc.* **15**, 1649 (2020).
42. Lloyd-Lewis, B. *et al.* Imaging the mammary gland and mammary tumours in 3D: Optical tissue clearing and immunofluorescence methods. *Breast Cancer Res.* **18**, 1–17 (2016).
43. Susaki, E. A. *et al.* Whole-brain imaging with single-cell resolution using chemical cocktails and computational analysis. *Cell* **157**, 726–739 (2014).
44. Md. Mahmudul Alam*, K. J. and D. P. Potential application of CuSO4 for the reduction of lipofuscin autofluorescence in formalin-fixed paraffin-embedded tissue. *Bioresearch Commun.* **2**, 170–174 (2016).
45. Sun, Y., Ip, P. &Chakrabartty, A. Simple Elimination of Background Fluorescence in Formalin-Fixed Human Brain Tissue for Immunofluorescence Microscopy. *J. Vis. Exp.* **2017**, 56188 (2017).
46. Zeller, P., Ploux, O. &Méjean, A. A simple protocol for attenuating the auto-fluorescence of cyanobacteria for optimized fluorescence in situ hybridization (FISH) imaging. *J. Microbiol. Methods* **122**, 16–19 (2016).
47. Pyon, W. S., Gray, D. T. &Barnes, C. A. An alternative to dye-based approaches to remove background autofluorescence from primate brain tissue. *Front. Neuroanat.* **13**, 73 (2019).
48. Wang, S. C., Hong, J. H., Hsueh, C. &Chiang, C. S. Tumor-secreted SDF-1 promotes glioma invasiveness and TAM tropism toward hypoxia in a murine astrocytoma model. *Lab. Invest.* **92**, 151–162 (2012).
49. Huang, G.-J. *et al.* Towards stimulated Raman scattering spectro-microscopy across the entire Raman active region using a multiple-plate continuum. *Opt. Express, Vol. 30, Issue 21, pp. 38975-38984* **30**, 38975–38984 (2022).
50. Todorov, M. I. *et al.* Machine learning analysis of whole mouse brain vasculature. *Nat. Methods 2020 174* **17**, 442–449 (2020).
51. Lee, T. C., Kashyap, R. L. &Chu, C. N. Building Skeleton Models via 3-D Medial Surface

Axis Thinning Algorithms. *CVGIP Graph. Model. Image Process.* **56**, 462–478 (1994).

Acknowledgments

We thank the Brain Research Center, National Tsing-Hua University, Taiwan and Pathology core, Institute of Biomedical Sciences, Academia Sinica, Taiwan for the technical assistance. This work was funded by the grants from National Science and Technology Council (NSTC-111-2636-B-007-007, NSTC-07-2314-B-007-003-MY3, NSTC-111-2321-B-002-016, MOST-110-2321-B-010-006, MOST-111-2636-B-007-007). This work was also supported by the Brain Research Center under the Higher Education Sprout Project, co-funded by the Ministry of Education and the National Science and Technology Council in Taiwan.

Author information

Contributions

Y.H.L., B.C.C. and L.A.C. conceived the study and designed the experiments. Y.H.C. prepared FFPE samples. Y.H.L. performed immunostaining, imaging and image visualization. Y.H.L. and L.W.W. performed image data analysis. Y.C.C. and S.H.H. provided TBI-induced mice. S.Y.W. and C.S.C. provided the tumor-implanted mice. S.D.Y. performed Raman microscopy. S.T.H., K.C.W., C.H.L. and H.J.C. provided the human brain tissues. Y.H.L. and L.A.C. wrote the manuscript.

Corresponding authors

Correspondence to Li-An Chu and Bi-Chang Chen

Ethics declarations

Competing interests

The authors declare no competing interests.

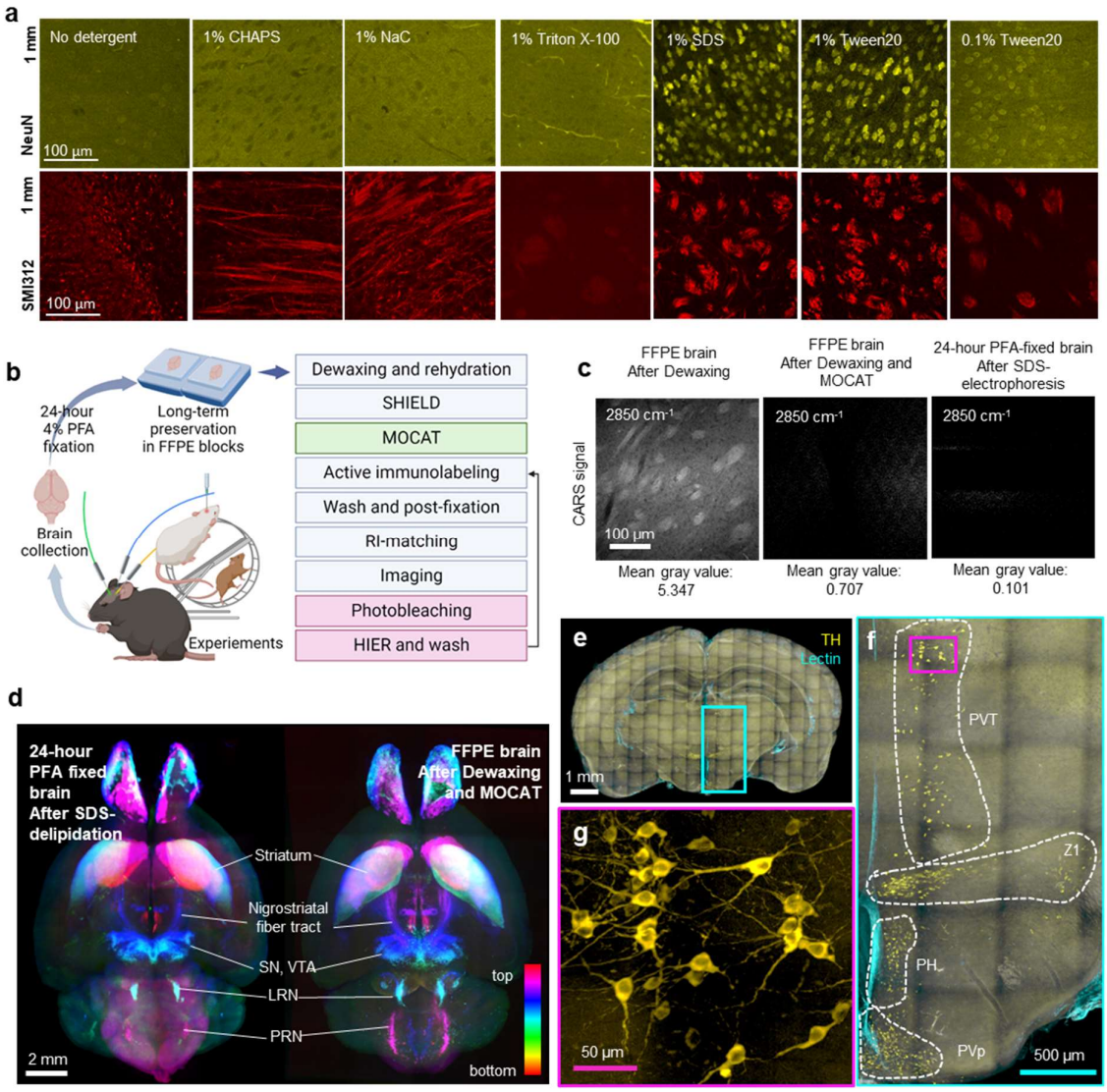

Fig. 1: MOCAT reveals the three-dimensional (3D) biomarker expression pattern of a whole FFPE mouse brain. a, Fluorescent images of neuronal nuclei (upper row) in the cortex and axons (bottom row) in the striatum from 2-mm thick FFPE mouse brain slices that were treated with various detergent conditions. Images of the optical section at 1 mm depth are shown. Detergent types and concentrations are indicated. NeuN, a neuronal nuclear marker; SMI312, a pan-axonal marker. **b,** The MOCAT workflow. **c,** Images of coherent anti-Stokes Raman scattering (CARS) of dewaxed FFPE mouse brain without antigen retrieval; dewaxed FFPE mouse brain with antigen retrieval and freshly prepared SDS-delipidated mouse brain. The images were taken at the Raman shift of 2850 cm^{-1} to address the CH2 vibration frequency. The mean gray values are shown below images. **d,** Brain-wide tyrosine hydroxylase (TH) expression in FFPE and fresh wild-type C57BL/6 mice. The expression patterns are shown in temporal code. The major dopaminergic regions are identified. SN, substantia nigra; VTA, ventral tegmental area; LRN, lateral reticular nucleus; PRN, pontine reticular nucleus. **e-g,** Application of MOCAT to a 15-year-old FFPE block. **e,** The projection image of a 2-mm-thick mouse brain slice retrieved from the 15-year-old FFPE block. **f,** Magnification of the region marked in **e.** The dopaminergic regions are identified. PVT, paraventricular nucleus of thalamus; PH, posterior

hypothalamic nucleus; PVp, periventricular hypothalamic nucleus. **g,** Magnification of the region marked in **e**. Scale bars are indicated on each figure.

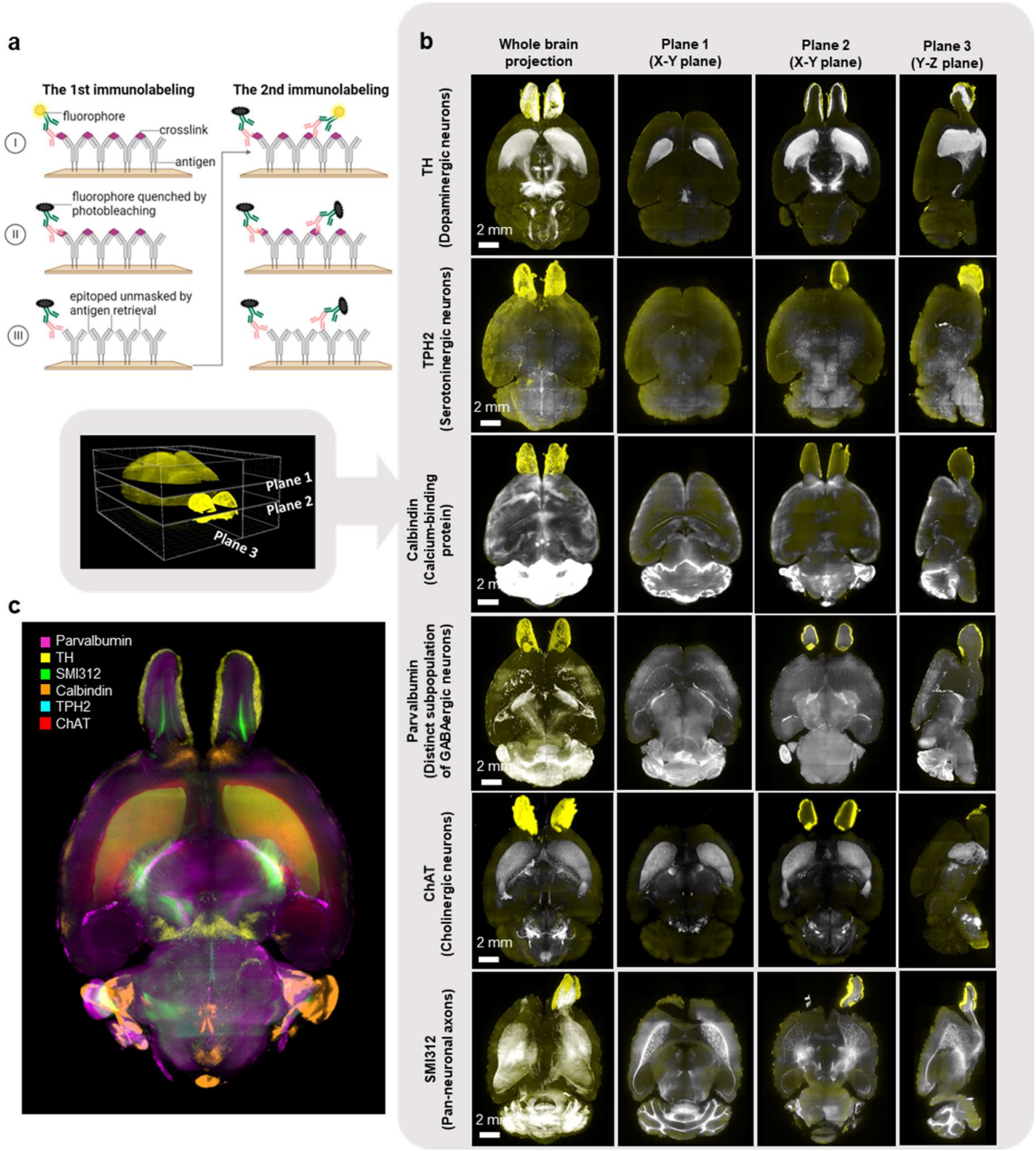

Fig. 2: MOCAT enables multiple rounds of whole-brain immunostaining. a, A schematic of the photobleaching and antigen retrieval steps. **b,** The image data sets of 6-round immunolabeling. Two X–Y planes (different z-positions) and one Y–Z plane are shown. **c,** The merged multichannel image.

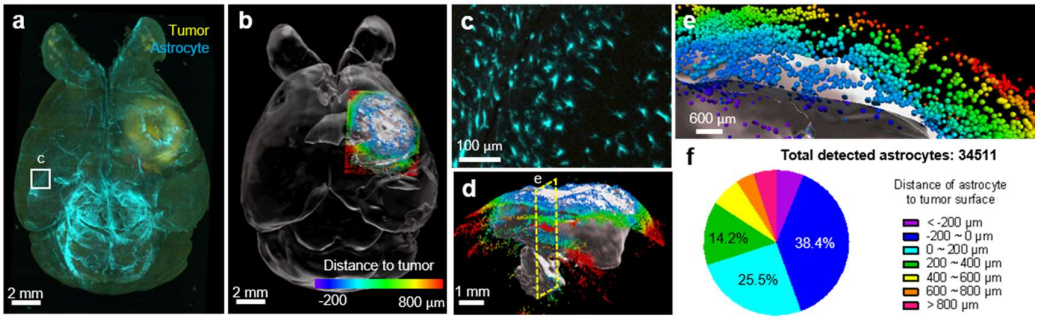

Fig. 3: MOCAT reveals cell-tumor relationship in an astrocytoma model. a, The projection image of a MOCAT-processed mouse brain with xenograft astrocytoma (ALTS1C1 cells, see Methods). **b,** Segmented mouse brain with tumor (white) and surrounding astrocytes. The astrocytes are colored in cell-to-tumor distance-code. **c,** The magnification of the region marked in **a**, showing the morphology of astrocytes. **d,** The sagittal view of the segmented tumor and color-coded astrocytes. **e,** The magnification of the clipping plane marked in **d**, showing astrocytes inside (dark blue, purple) and outside the tumor. **f,** Quantification of the detected astrocytes and classification according to their distance to tumor surface.

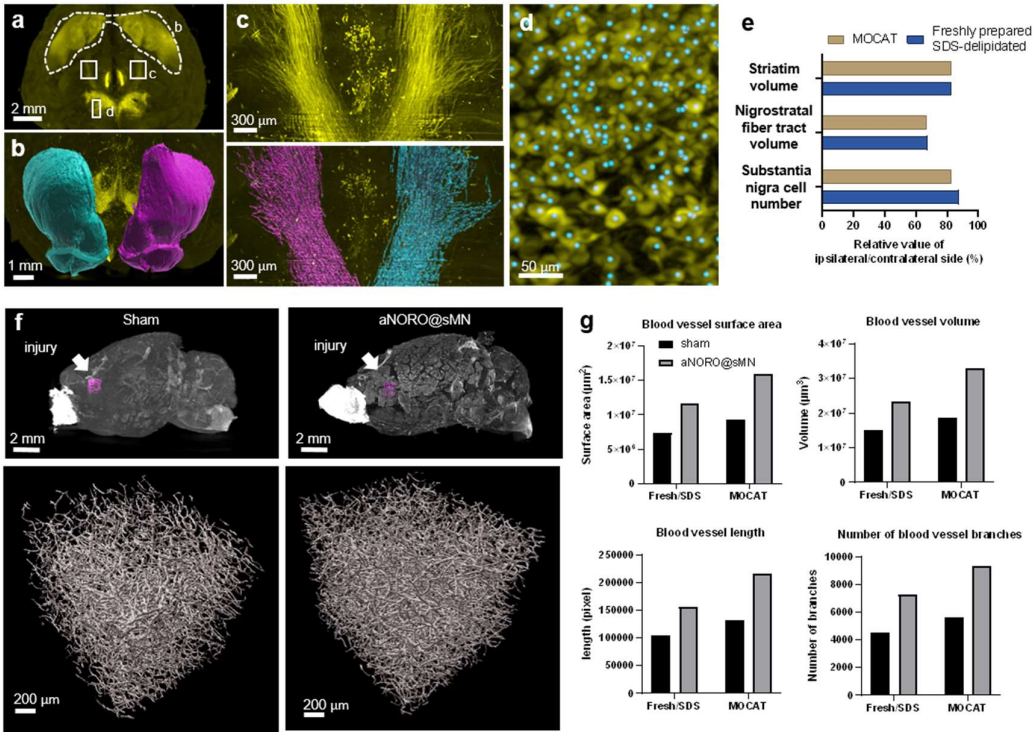

Fig. 4: MOCAT demonstrates damage and therapeutic effect of NO-released particles in TBI mouse model. a, Fluorescent image of TH immunolabeling. **b,** Frontal view of segmented striatum (dot line circled in **a**). Magenta: the injury side; cyan: the contralateral side. **c,** The horizontal views of the nigrostriatal fiber tract (marked in **a**); fluorescent and segmented images are shown (upper and bottom in order). Magenta: the injury side; cyan: the contralateral side. **d,** Detection of dopaminergic cells in substantia nigra (SN). Magnification of the marked area in **a**, including the original TH fluorescent signal (yellow) and segmented cell spots (cyan dots), is shown. **e,** Quantification of striatum volume, nigrostriatal volume, and substantia nigra cell number. The relative ipsilateral/contralateral values are shown. **f,** Reconstruction of blood vessels in TBI brains with and without treatments. The regions of interested (ROIs) selected for assessment of angiogenesis were indicated in the upper row (magenta boxes, right below the injury site). The 3D reconstructions of blood vessels were shown in the bottom row. **g,** Quantification of blood vessel volume, blood vessel surface area, number of blood vessel branches, and blood vessel length. Both of the MOCAT- and SHIELD-processed aNORO@sMN-treated group (see Methods) shows approximately 60% improvements compared with the sham group.

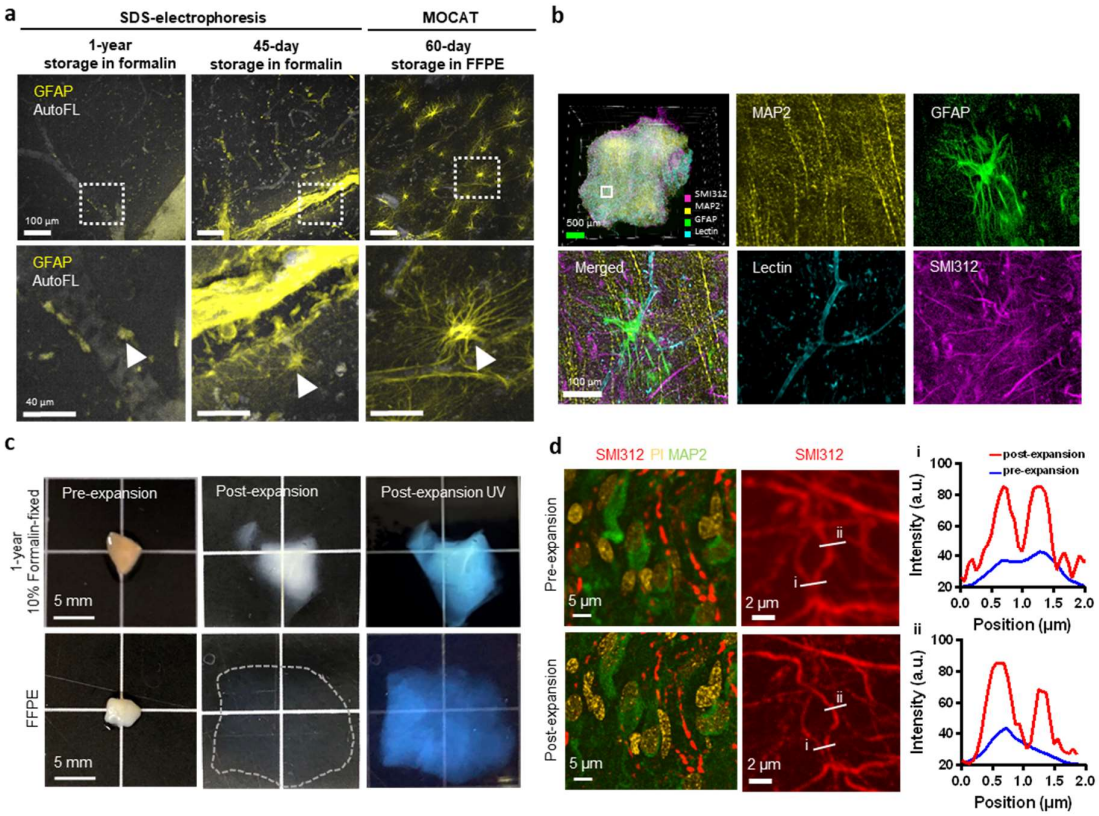

Fig. 5: Application of MOCAT to human brain tissue. a, Fluorescent images of human brain tissues Immunolabeled with glial fibrillary acidic protein (GFAP; the astrocyte marker). Human brain tissues stored in formalin or FFPE blocks are cleared by SDS-electrophoresis or MOCAT before immunbolabeling. The bottom row shows magnification of the boxed regions in the upper row. Stained astrocytes are indicated by arrowheads. **b,** Multiplexed immunolabeling of an FFPE human brain tissue using MOCAT. The 3D reconstruction of the whole tissue, and the images of merged and single channels of one optical section of the selected area (white box) are shown. GFAP: Glial fibrillary acidic protein; SMI312: pan-axonal marker; MAP2: microtubule-associated protein 2, a dendritic marker. **c,** Pre- and post-expansion bright-field images of 1-year formalin-fixed human brain tissue and FFPE brain tissue. The post-expansion FFPE human tissue is outlined with a dashed line. Tissue existence are demonstrated by UV. **d,** Fluorescent images of pre- (upper row) and post-expansion (bottom row) FFPE human brain. Left: The merged images of multiplexed staining; middle: Fluorescent images of SMI312 staining; right: The profiles of axon intensity taken along the line in images of the middle column. The scale bar is divided by the expansion factor.